

CEBAF-TH-93-04 / MIT-CTP-2187 / ORNL-CCIP-93-01

## NN Core Interactions and Differential Cross Sections from One Gluon Exchange

T.Barnes

*Physics Division and Center for Computationally Intensive Physics  
Oak Ridge National Laboratory, Oak Ridge, TN 37831-6373  
and*

*Department of Physics  
University of Tennessee, Knoxville, TN 37996-1200*

S.Capstick

*Continuous Electron Beam Accelerator Facility  
12000 Jefferson Ave., Newport News, VA 23606*

M.D.Kovarik

*Physics Division and Center for Computationally Intensive Physics  
Oak Ridge National Laboratory, Oak Ridge, TN 37831-6373  
and*

*University of Tennessee Computer Center  
University of Tennessee, Knoxville, TN 37996-0520*

E.S.Swanson

*Center for Theoretical Physics  
Laboratory of Nuclear Science and Department of Physics  
Massachusetts Institute of Technology, Cambridge, MA 02139*

We derive nonstrange baryon-baryon scattering amplitudes in the nonrelativistic quark model using the “quark Born diagram” formalism. This approach describes the scattering as a single interaction, here the one-gluon-exchange (OGE) spin-spin term followed by constituent interchange, with external nonrelativistic baryon wavefunctions attached to the scattering diagrams to incorporate higher-twist wavefunction effects. The short-range repulsive core in the NN interaction has previously been attributed to this spin-spin interaction in the literature; we find that these perturbative constituent-interchange diagrams do indeed predict repulsive interactions in all I,S channels of the nucleon-nucleon system, and we compare our results for the equivalent short-range potentials to the core potentials found by other authors using nonperturbative methods. We also apply our perturbative techniques to the  $N\Delta$  and  $\Delta\Delta$  systems: Some  $\Delta\Delta$  channels are found to have attractive core potentials and may accommodate “molecular” bound states near threshold. Finally we use our

Born formalism to calculate the NN differential cross section, which we compare with experimental results for unpolarised proton-proton elastic scattering. We find that several familiar features of the experimental differential cross section are reproduced by our Born-order result.

February 1993

## I. INTRODUCTION

The nucleon-nucleon interaction exhibits a strongly repulsive short-distance core and a longer-ranged but much weaker attraction. Although there has been evidence of the general features of this interaction for over fifty years [1], the physical mechanisms proposed as the origin of the interaction have changed as our understanding of the strong interaction has progressed. In 1935 Yukawa [2] suggested that the finite-ranged nuclear attraction was due to the exchange of a massive, strongly-interacting meson, by analogy with electron sharing as the origin of chemical forces. This hypothetical meson was identified with the pion after its discovery, and as the lightest hadron it certainly contributes the longest-ranged component of the nucleon-nucleon strong force. The repulsive short-range core of the nucleon-nucleon interaction was similarly attributed to the exchange of heavier mesons such as the  $\omega$  after their discovery. These meson-exchange models have been elaborated considerably since these original suggestions, and the most accurate phenomenological descriptions of the nucleon-nucleon interaction at present are meson exchange models [3], with parameters such as meson-nucleon couplings fitted to experiment.

A literal attribution of the short-range repulsive core to vector meson exchange, as opposed to a phenomenological parametrization, of course involves a *non sequitur* [4,5]: Since the nucleons have radii of  $\approx 0.8$  fm, and the range of the vector-exchange force is  $1/m_\omega \approx 0.2$  fm, one would have to superimpose the nucleon wavefunctions to reach the appropriate internucleon separations. The picture of distinct nucleons exchanging a physical  $\omega$  meson at such a small separation is clearly a fiction, and a realistic description of the short-range core interaction requires a treatment of the quark wavefunctions of the interacting nucleons and a Hamiltonian which involves quark and gluon degrees of freedom.

Since the development of QCD as the theory of the strong interaction there have been many studies of the NN interaction in terms of quarks and gluons. Most have employed the nonrelativistic quark potential model, although some early work used the MIT bag model [6]. Many studies of this and other multiquark systems were fundamentally flawed due to an inadequate treatment of the color degree of freedom, or due to assumptions that imposed confinement on the entire multiquark system; a discussion of these problems is given by Isgur [4]. It now appears that a pairwise  $\lambda \cdot \lambda$  color interaction [7–9] together with a sufficiently general spatial wavefunction that allows dissociation into color singlets provides a sufficiently realistic description of color forces in a multiquark system. The NN references summarised here all assume the  $\lambda \cdot \lambda$  form, and it has also become standard to employ a quadratic or linear confinement potential. Finally, the spin-spin hyperfine term is incorporated in all these references, as it apparently makes a dominant contribution to the NN core interaction. Several groups have included other terms from the Breit-Fermi interaction such as the hyperfine-tensor and spin-orbit interactions.

Attempts to describe the NN interaction using quark potential models date from the work of Liberman in 1977 [10], who calculated the adiabatic response of the six quark system to variations in the interbaryon coordinate. The resulting effective potential had a repulsive core with a weak intermediate-range attraction. Liberman concluded that the repulsive core was predominantly due to a combination of the Pauli principle and the contact hyperfine term. The same conclusion was reached by Neudatchin and collaborators [11], also within the adiabatic approximation. Harvey [12] continued this adiabatic approach in a generalized

calculation of the effective NN potential; he noted that SU(4) spin-isospin symmetry required that NN,  $\Delta\Delta$ , and “hidden color”  $(qqq)_8 \otimes (qqq)_8$  states be included in the calculation. On incorporating these states, he found that the repulsive core was strongly suppressed. It is now widely believed that the absence of the repulsive core in improved calculations is an artifact of the adiabatic approximation [13,14].

The usual method for improving on the adiabatic approximation in the  $q^6$  system is to employ the resonating-group method. This involves expanding the wavefunction of the system in a basis which describes system subclusters multiplied by unknown functions of the intercluster coordinates. One then solves the resulting coupled integro-differential equations using various numerical techniques. Baryon subcluster wavefunctions are usually taken to be simple Gaussians, and the coupled system is truncated at the NN, NN +  $\Delta\Delta$ , or NN +  $\Delta\Delta$  + hidden color levels. The first applications of the resonating-group method to the NN system were given by Warke and Shanker [15], Oka and Yazaki [16] and Ribeiro [17]. All groups found a repulsive core, which was dominantly due to the Pauli principle and the color hyperfine term. The  $\Delta\Delta$  and hidden color channels were found to make only small contributions to the hard-core S-wave phase shifts. These studies found that several contributions including the Coulomb and confinement kernels approximately cancelled, leaving the spin-spin OGE hyperfine term as the dominant interaction. The resonating-group approach has been extended to include more channels, strange quarks, effective one-boson-exchange long-range potentials, and virtual excitations of the quark wavefunctions. In particular, Koike [18] has applied these techniques to the “flip-flop” model [19] (which eliminates long-range color van der Waals forces), supplemented by an effective meson-exchange potential, and Cao and Kisslinger [20] have developed a relativised resonating-group formalism and applied it to the determination of equivalent potentials and low-L phase shifts in a model which incorporates OGE and meson exchange forces. Both these references find reasonably good agreement with experimental low-energy NN phase shifts. A summary of work in this field to 1989 has been given by Shimizu [21].

Maltman and Isgur [22] have performed a detailed variational calculation of the ground state properties of the deuteron using a  $\lambda \cdot \lambda$  quark-quark interaction with the full OGE color Breit-Fermi interaction, a quadratic confinement term, and a phenomenological one-pion-exchange potential. In contrast to typical resonating-group calculations, they allowed spatial excitations within the clusters. They found a repulsive core, and noted that the admixture of P-wave color octet clusters significantly increased the range and depth of the intermediate-range attraction. Their results for the deuteron binding energy, RMS radius, quadrupole moment, and magnetic moment all agreed well with experiment.

Although the origin of the nucleon-nucleon force at the QCD level is now reasonably well understood, the resonating-group and variational techniques which have been employed in this work are rather intricate and require considerable theoretical effort, and usually lead to numerical rather than analytical results. As these techniques are best suited to the determination of ground state properties, topics such as resonance production and scattering cross sections at higher energies have received little attention in these quark model studies.

In recent work we have investigated the possibility that these low-energy nonresonant hadronic scattering amplitudes may actually be dominated by simple perturbative processes; if so, it may be possible to derive useful estimates of these amplitudes using a much simpler approach. A complementary possibility of perturbative dominance of hadronic scattering

processes at high energies through constituent-interchange mechanisms has been investigated by theorists almost since the development of QCD [23]. Results for elastic hadron-hadron scattering amplitudes, in particular the asymptotic  $Q^2$  dependence of fixed-angle scattering, have recently been presented by Botts and Sterman [24].

Concerns regarding the range of validity of the high-energy perturbative QCD studies have been expressed by Isgur and Llewellyn-Smith [25], who suggest that higher-twist hadron wavefunction effects may actually dominate perturbative QCD contributions at experimentally accessible energies. We have explicitly incorporated these wavefunction effects in our study of a constituent-interchange scattering mechanism in the nonrelativistic quark potential model. We calculate the hadron-hadron scattering amplitudes which follow from one gluon exchange followed by constituent interchange (quark line interchange is required at lowest order in  $\alpha_s$  to restore color singlet final states), with nonrelativistic quark model wavefunctions attached to the external lines. This OGE+CI mechanism may be dominant in processes in which  $q\bar{q}$  annihilation is forbidden for the valence wavefunctions. We have applied this description of scattering to elastic  $I=2 \pi\pi$  [26] and  $I=3/2 K\pi$  [27] reactions and found excellent agreement with the experimental S-wave phase shifts given standard quark model parameters. Related approaches to calculating meson-meson scattering amplitudes which iterate this quark-gluon mechanism have been discussed in the literature [28]. These Born-order techniques have also been applied to vector-vector meson systems [29], and lead to interesting predictions of vector-vector molecule bound states in certain channels [30]. In the vector-vector system the hyperfine interaction apparently does not dominate the scattering amplitude, unlike the pseudoscalar-pseudoscalar and NN systems. More recently we applied the quark Born formalism to KN scattering [31], which is also free of  $q\bar{q}$  annihilation at the valence quark level. We found satisfactory agreement with the experimental S-wave KN scattering lengths, although  $I=0$  is not yet very well determined experimentally. The KN S-wave phase shifts at higher energies, however, are not well described; they require stronger high-momentum components in the nucleon wavefunction than are present in the single Gaussian forms we assumed. The higher-L KN partial waves, especially the P-waves, show evidence of a spin-orbit interaction which does not arise in single-channel spin-spin scattering, which has not yet been adequately explained in the literature.

The next level of complexity in Hilbert space is the  $q^6$  baryon-baryon sector. Since this system is free of annihilation at the valence level, and the spin-spin hyperfine term has already been established as the dominant interaction underlying the core repulsion, derivation of the NN core interaction is an important test of the quark Born formalism. Here we derive the nucleon-nucleon interaction predicted by the OGE spin-spin term using quark Born diagrams, and show that the predicted core interaction is indeed strongly repulsive in all four spin and isospin channels. Low energy Born-equivalent NN core potentials are also derived and compared to previous results. We then consider other nonstrange baryons and derive the  $N\Delta$  and  $\Delta\Delta$  short-range interactions; some of these are found to be attractive, and we investigate the possibility that these channels might support dibaryon molecule bound states. Some of our results for attractive  $\Delta\Delta$  channels are consistent with the previous conclusions of Maltman [32]. Finally we derive the elastic NN differential cross section predicted by our quark Born formalism and find that some familiar experimental features of the high-energy elastic proton-proton differential cross section are evident in our results.

## II. DERIVATION OF SCATTERING AMPLITUDES

### a) Hamiltonian and hadron states

In the quark Born diagram formalism we derive the matrix element of the interaction Hamiltonian between quarks in incoming hadron states to leading Born order, which is then used to calculate scattering observables. We factor out the overall momentum conserving delta function and then derive the remaining matrix element, which we call  $h_{fi}$ ;

$$_f\langle BB'|H_{scat}|BB'\rangle_i \equiv h_{fi} \delta(\vec{P}_f - \vec{P}_i) . \quad (1)$$

Since the hadron state normalizations we will introduce are identical to those used in our previous study of  $I=2 \pi\pi$  scattering [26] we can use the relations between the scattering matrix element  $h_{fi}$  and the phase shifts and cross sections given there. The details of our diagrammatic procedure for determining  $h_{fi}$  are described elsewhere [26,27,31]; here we shall simply recall some basic points and then give our results.

For baryon-baryon scattering we shall follow previous studies [4,10–19,21,22] and assume that the dominant part of the core interaction derives from the spin-spin color hyperfine term,

$$H_{scat} = \sum_{a,i < j} \left[ -\frac{8\pi\alpha_s}{3m_i m_j} \delta(\vec{r}_{ij}) \right] \left[ \vec{S}_i \cdot \vec{S}_j \right] \left[ \mathcal{F}_i^a \cdot \mathcal{F}_j^a \right] , \quad (2)$$

where  $\mathcal{F}_i^a$  is the color matrix  $\lambda^a/2$  for quark  $i$ . The baryon color wavefunctions are the usual color singlets,

$$|baryon\rangle = \sum_{i,j,k=1,3} \frac{1}{\sqrt{6}} \epsilon_{ijk} |ijk\rangle . \quad (3)$$

Our spin-flavor states for the meson and baryon are the usual SU(6) states, but as explained in reference [31] we find it convenient to write these states using field theory conventions rather than in the usual quark model form. The quark model conventions show explicit exchange symmetry by assigning a fixed location in the state vector to each quark. The field theoretic convention greatly reduces the number of terms encountered in our scattering matrix elements; for example, the proton state in field theory conventions has only 2 terms instead of the usual 9 for quark model states, so  $PP \rightarrow PP$  elastic scattering involves only 16 terms, far fewer than the 6561 we would encounter with the usual quark model conventions. As examples, the orthonormal  $S_z = 3/2 |\Delta_{3/2}^+\rangle$  and  $S_z = 1/2 |P_{1/2}\rangle$  states in field theory conventions are

$$|\Delta_{3/2}^+\rangle = \frac{1}{\sqrt{2}} |u_+ u_+ d_+\rangle \quad (4)$$

and

$$|P_{1/2}\rangle = \sqrt{\frac{2}{3}} \left\{ \frac{|u_+ u_+ d_-\rangle}{\sqrt{2}} \right\} - \sqrt{\frac{1}{3}} |u_+ u_- d_+\rangle . \quad (5)$$

The other baryon states considered in this paper can be derived from these by application of spin and isospin raising and lowering operators.

We shall quote general results for baryon-baryon scattering amplitudes with arbitrary spatial wavefunctions attached to the external lines and then specialize to single-Gaussian forms to derive representative closed-form results. The general spatial baryon wavefunction we assume is of the form

$$\Phi_{baryon}(\vec{p}_1, \vec{p}_2, \vec{p}_3; \vec{P}_{tot}) = \phi_{baryon}(\vec{p}_1, \vec{p}_2, \vec{p}_3) \delta(\vec{P}_{tot} - \vec{p}_1 - \vec{p}_2 - \vec{p}_3) \quad (6)$$

with a normalization given by

$$\begin{aligned} & \langle \Phi_{baryon}(\vec{P}'_{tot}) | \Phi_{baryon}(\vec{P}_{tot}) \rangle \\ &= \int \int \int \int \int \int d\vec{p}_1 d\vec{p}_2 d\vec{p}_3 d\vec{p}_1' d\vec{p}_2' d\vec{p}_3' \Phi_{baryon}^*(\vec{p}_1', \vec{p}_2', \vec{p}_3'; \vec{P}'_{tot}) \Phi_{baryon}(\vec{p}_1, \vec{p}_2, \vec{p}_3; \vec{P}_{tot}) \\ &= \delta(\vec{P}_{tot} - \vec{P}'_{tot}) . \end{aligned} \quad (7)$$

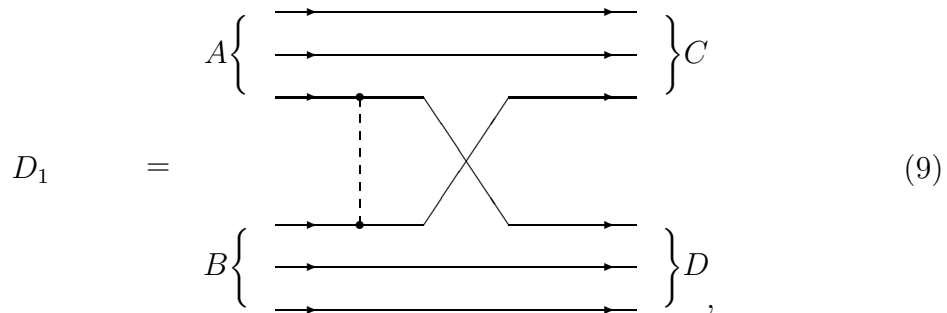
The standard quark model single-Gaussian baryon wavefunction we shall use for illustration is

$$\phi_{baryon}(\vec{p}_1, \vec{p}_2, \vec{p}_3) = \frac{3^{3/4}}{\pi^{3/2} \alpha^3} \exp \left\{ - \frac{(\vec{p}_1^2 + \vec{p}_2^2 + \vec{p}_3^2 - \vec{p}_1 \cdot \vec{p}_2 - \vec{p}_2 \cdot \vec{p}_3 - \vec{p}_3 \cdot \vec{p}_1)}{3\alpha^2} \right\} . \quad (8)$$

Oscillator parameter values of  $0.25 \text{ GeV} \leq \alpha \leq 0.42 \text{ GeV}$  have been used in the quark model literature on baryon spectroscopy, as we will discuss subsequently.

### b) Baryon-baryon scattering amplitudes

By analogy with our study of KN scattering [31] (see especially section IIb) we first write a generic scattering diagram with initial and final baryon-baryon states. We then connect the initial and final quark lines in all ways consistent with flavor conservation; for example  $\Delta^{++}\Delta^{++}$  elastic scattering has  $6!=720$  quark line diagrams. These may be grouped into four sets in which the number of  $q\bar{q}$  pairs which cross in t-channel is zero, one, two or three. We then generate scattering diagrams by inserting one-gluon-exchange interactions between all pairs of initial quarks in different initial baryons; this gives nine times as many scattering diagrams as we had quark line diagrams. Many of these diagrams are trivially zero; these include the zero-pair-interchange and three-pair-interchange diagrams, which vanish due to color. The nonzero scattering diagrams may be related to a small “reduced set” of diagrams by permutation of external lines, which leaves a diagram invariant. In baryon-baryon scattering this reduced set contains eight independent diagrams, which are shown below.



$$D_2 = \text{Diagram} \quad , \quad (10)$$

$$D_3 = \begin{array}{c} \text{Diagram of } D_3 \text{ with two horizontal lines and a central crossing} \\ \text{Diagram of } D_3 \text{ with two horizontal lines and a central crossing} \\ \text{Diagram of } D_3 \text{ with two horizontal lines and a central crossing} \end{array} , \quad (11)$$

$$D_4 = \text{Diagram} \quad , \quad (12)$$

$$D_5 = \text{Diagram} \quad (13)$$

$$D_6 = \begin{array}{c} \text{Diagram } D_6 \text{ is a spatial overlap integral with 6 external lines. It consists of a vertical dashed line with two dots. Two horizontal lines enter from the left, cross the dashed line, and exit to the right. Two other horizontal lines enter from the left, cross the dashed line, and exit to the right. The lines are labeled with arrows indicating direction. The diagram is enclosed in a box with a comma at the bottom.} \end{array} , \quad (14)$$

$$D_7 = \begin{array}{c} \text{Diagram } D_7 \text{ is a spatial overlap integral with 7 external lines. It consists of a vertical dashed line with two dots. Three horizontal lines enter from the left, cross the dashed line, and exit to the right. The lines are labeled with arrows indicating direction. The diagram is enclosed in a box with a comma at the bottom.} \end{array} , \quad (15)$$

$$D_8 = \begin{array}{c} \text{Diagram } D_8 \text{ is a spatial overlap integral with 8 external lines. It consists of a vertical dashed line with two dots. Four horizontal lines enter from the left, cross the dashed line, and exit to the right. The lines are labeled with arrows indicating direction. The diagram is enclosed in a box with a comma at the bottom.} \end{array} . \quad (16)$$

In a given baryon-baryon scattering process the matrix element  $h_{fi}$  in (1) is a weighted sum of the eight spatial overlap integrals represented by the diagrams  $D_1 \dots D_8$ ,

$$h_{fi} = \sum_{n=1}^8 w_n I_n(D_n) . \quad (17)$$

The weight of each diagram (introduced in [31]) is the product of a color factor, a fermion permutation phase called the “signature” of the diagram (which is  $-1$  for  $D_1 \dots D_4$  and  $+1$  for  $D_5 \dots D_8$ ), the overall  $(-)$  in  $H_I$  (2), and a reaction-dependent spin-flavor factor. The derivation of these factors and the spatial overlap integrals they multiply is discussed in detail elsewhere [26,31], so here we will simply present results with minimal discussion. There is a minor change in the convention for diagram weights relative to our earlier reference. In our KN study [31] we incorporated the  $(-)$  phase of  $H_I$  and the signature phase in the spatial overlap integral; here we include them in the diagram weight. This overall factor was  $(+1)$  for all KN diagrams, so the KN weights are unchanged by our new convention. Similarly, in our first paper [26] we incorporated the  $(-)$  phase of  $H_I$  in the spatial overlap integral. Our

new convention is useful because it makes all the NN spatial overlap integrals considered here positive, so the overall amplitude phases are clear from the weights alone.

The color factors of the diagrams  $D_1 \dots D_8$  are

$$I_{color}([D_1 \dots D_8]) = [ +4/9, -2/9, -2/9, +1/9, +4/9, -2/9, -2/9, +1/9 ]. \quad (18)$$

$D_n$  is related to  $D_{n+4}$  by  $t \leftrightarrow u$  crossing; for this reason the weights  $w_n$  and  $w_{n+4}$  are closely related in many reactions. To simplify our presentation, when possible we will just give results for the weights of  $D_1 \dots D_4$  and indicate the relative phase of the set for  $D_5 \dots D_8$  after a bar. Thus for  $\{I_{color}(D_n)\}$  above we write

$$I_{color} = [ +4/9, -2/9, -2/9, +1/9 | (+) ]. \quad (19)$$

The spin-flavor weights (incorporating the signature phases) are just matrix elements of the operator  $\vec{S}_i \cdot \vec{S}_j$  between two initial quarks for the given process. As an example, for  $\Delta^{++}\Delta^{++}$ ,  $S = 3, S_z = 3$  scattering there are four  $|u_+u_+u_+\rangle/\sqrt{6}$  external baryons, and only the  $S_i^z S_j^z$  terms contribute. On summing over all scattering diagrams in this channel we find

$$I_{spin-flavor} \cdot I_{signature} \Big|_{\Delta\Delta, I=3, S=3} = [ +9/4, +9/2, +9/2, +9 | (-) ], \quad (20)$$

which is  $I_z$ - and  $S_z$ -independent. Combining these we find the  $I = 3, S = 3$   $\Delta\Delta$  diagram weights,

$$\{w_n(\Delta\Delta, I = 3, S = 3)\} = [ +1, -1, -1, +1 | (-) ]. \quad (21)$$

Since the spatial overlap integrals  $I_5(D_5) \dots I_8(D_8)$  are equal to the integrals  $I_1(D_1) \dots I_4(D_4)$  after  $t \leftrightarrow u$  crossing, the relative  $(-)$  phase in the diagram weights (21) insures that the  $I = 3, S = 3$   $\Delta\Delta$  scattering amplitude  $h_{fi}$  is spatially antisymmetric, as required for a totally antisymmetric fermion-fermion scattering amplitude that is symmetric in the remaining degrees of freedom (I and S). This antisymmetry is a nontrivial check of our spin-flavor combinatorics, since it is only evident after the sum over individual quark-gluon scattering diagrams is completed.

The diagram weights for all I,S channels of NN,  $N\Delta$  and  $\Delta\Delta$  elastic scattering are tabulated at the end of the paper; these and the overlap integrals constitute our central results.

The spatial overlap integrals associated with the diagrams may be determined using the simple diagrammatic techniques presented in Appendix C of reference [26]. In these integrals all momenta are implicitly three-dimensional, and have an overall spin-spin coefficient  $\kappa_{ss}$  of

$$\kappa_{ss} = \frac{8\pi\alpha_s}{3m_q^2} \frac{1}{(2\pi)^3}. \quad (22)$$

This is  $(-1)$  times the  $\kappa$  of [26], since we have chosen to include the  $(-)$  phase of  $H_I$  (2) in the diagram weight factor, as discussed above. The integrals are

$$I_1 = \kappa_{ss} \iint da_1 da_2 \Phi_A(a_1, a_2, A - a_1 - a_2) \Phi_C^*(a_1, a_2, C - a_1 - a_2)$$

$$\cdot \iint db_2 db_3 \Phi_B(-A - b_2 - b_3, b_2, b_3) \Phi_D^*(-C - b_2 - b_3, b_2, b_3) ; \quad (23)$$

$$I_2 = \kappa_{ss} \iiint da_1 da_3 db_2 dc_3 \Phi_A(a_1, A - a_1 - a_3, a_3) \Phi_C^*(a_1, C - a_1 - c_3, c_3) \Phi_B(C - A + a_3, b_2, -C - a_3 - b_2) \Phi_D^*(a_3, b_2, -C - a_3 - b_2) ; \quad (24)$$

$$I_3 = \kappa_{ss} \iiint da_1 da_2 db_3 dd_1 \Phi_A(a_1, a_2, A - a_1 - a_2) \Phi_C^*(a_1, a_2, C - a_1 - a_2) \Phi_B(C - a_1 - a_2, -A - C + a_1 + a_2 - b_3, b_3) \Phi_D^*(d_1, -C - b_3 - d_1, b_3) ; \quad (25)$$

$$I_4 = \kappa_{ss} \iiint da_1 da_3 db_1 db_3 \Phi_A(a_1, A - a_1 - a_3, a_3) \Phi_C^*(a_1, C - a_1 - b_1, b_1) \Phi_B(b_1, -A - b_1 - b_3, b_3) \Phi_D^*(a_3, -C - a_3 - b_3, b_3) . \quad (26)$$

We evaluate these in the c.m. frame, so the  $t \leftrightarrow u$  crossed integrals  $I_5 \dots I_8$  can be obtained by exchanging  $\vec{C}$  and  $\vec{D} = -\vec{C}$ , or in terms of the cosine of the c.m. scattering angle  $\mu = \cos(\theta_{\text{c.m.}})$ ,

$$I_{n+4}(\mu) = I_n(-\mu) . \quad (27)$$

A simplification follows if all baryons have the same spatial wavefunctions, as we assume here; in this case  $I_2 = I_3$  and hence  $I_6 = I_7$ .

The overlap integrals may be carried out in closed form given single-Gaussian wavefunctions (8), and each gives a result of the form

$$I_n = \kappa_{ss} \eta_n \exp \left\{ - (A_n - B_n \mu) P^2 \right\} , \quad (28)$$

where  $P$  is the magnitude of the c.m. three-momentum of each baryon,  $P^2 = \vec{A}^2 = \vec{B}^2 = \vec{C}^2 = \vec{D}^2$ . The results are

$$I_1 = \kappa_{ss} \exp \left\{ - \frac{1}{3\alpha^2} (\vec{A} - \vec{C})^2 \right\} = \kappa_{ss} \exp \left\{ - \frac{1}{3\alpha^2} 2(1 - \mu) P^2 \right\} = \kappa_{ss} \exp \left\{ \frac{t}{3\alpha^2} \right\} ; \quad (29)$$

$$I_2 = I_3 = \kappa_{ss} \left( \frac{12}{11} \right)^{3/2} \exp \left\{ - \frac{1}{33\alpha^2} (20 - 12\mu) P^2 \right\} \\ = \kappa_{ss} \left( \frac{12}{11} \right)^{3/2} \exp \left\{ - \frac{2(s - 4M^2)}{33\alpha^2} \right\} \exp \left\{ \frac{2t}{11\alpha^2} \right\} ; \quad (30)$$

$$I_4 = \kappa_{ss} \left( \frac{3}{4} \right)^{3/2} \exp \left\{ - \frac{1}{3\alpha^2} P^2 \right\} = \kappa_{ss} \left( \frac{3}{4} \right)^{3/2} \exp \left\{ - \frac{(s - 4M^2)}{12\alpha^2} \right\}. \quad (31)$$

In the final expression for each integral we have substituted for  $P^2$  and  $\mu$  in terms of the Mandelstam variables  $s$  and  $t$  using relativistic kinematics,  $s = 4(P^2 + M^2)$  and  $t = -2(1 - \mu)P^2$ .

Near threshold the overlap integrals are comparable in magnitude, but at higher energies their behaviors differ markedly. All but  $I_1$  and its crossing-symmetric partner  $I_5$  are strongly suppressed in  $s$ ; the diagrams  $D_1$  and  $D_5$  therefore dominate at high energies, for forward and backward scattering respectively. This behavior is due to the mechanism of “minimum spectator suppression”, as was discussed in detail in section IIe of reference [31]. To summarize the arguments for this case: 1) for forward scattering,  $\vec{A} = \vec{C}$ , diagram  $D_1$  (9) requires no spectator to cross into an opposite-momentum hadron, which would carry considerable suppression due to a small wavefunction overlap; only the hard-scattered constituents are required to reverse momentum. 2)  $D_5$  (13) requires all spectators that were initially in a baryon with momentum  $\vec{A}$  to reside finally in a baryon with momentum  $\vec{D}$ . Clearly the suppression due to wavefunction overlaps of the spectators will be less important if the final baryon  $D$  has the same momentum as the initial baryon  $A$ ,  $\vec{D} = \vec{A}$ . This corresponds to backscatter,  $\vec{C} = -\vec{A}$ , since  $\vec{C} = -\vec{D}$  in the c.m. frame. As in  $D_1$ , only the hard-scattered quarks are then required to recoil into a baryon with three-momentum opposite to that of their initial baryon. These two explanations are actually equivalent because  $D_1$  and  $D_5$  are related by crossing.

### III. NN CORE POTENTIALS AND PHASE SHIFTS

The Hamiltonian matrix elements

$$h_{fi} = \sum_{n=1}^8 w_n I_n \quad (32)$$

for the four I,S channels accessible in NN scattering are summarised by the diagram weights in Table I. Specialising to the even-L channels I,S=0,1 and 1,0, for which a repulsive core in S-wave is a well known feature, we see that all eight coefficients  $\{w_1 \dots w_8\}$  are positive or zero in both cases, corresponding to a repulsive interaction. For a more quantitative evaluation, we can relate this  $h_{fi}$  matrix element to an NN potential near threshold, which is defined to give the same low-energy scattering amplitude near threshold in Born approximation. (See Appendix E of reference [26] for a detailed discussion.) For an  $h_{fi}$  of the form

$$h_{fi} = \frac{8\pi\alpha_s}{3m_q^2} \frac{1}{(2\pi)^3} \sum_{n=1}^4 w_n \eta_n \exp \left\{ - (A_n - B_n \mu) P^2 \right\} \quad (33)$$

the Born-equivalent potential is

$$V_{NN}(r) = \frac{8\alpha_s}{3\sqrt{\pi}m_q^2} \sum_{n=1}^4 \frac{w_n \eta_n}{(A_n + B_n)^{3/2}} \exp \left\{ - \frac{r^2}{(A_n + B_n)} \right\}. \quad (34)$$

The  $t \leftrightarrow u$  crossed diagrams  $D_5 \dots D_8$  are not included in this sum because they will automatically be generated by the crossed diagram in NN $\rightarrow$ NN potential scattering through  $V_{NN}(r)$ .

The numerical potentials predicted for S-wave I=0 and I=1 NN systems are shown in Fig.1 for our “reference” set of quark model parameters [31],  $\alpha_s = 0.6$ ,  $m_q = 0.33$  GeV and  $\alpha = 0.4$  GeV. Actually only the two parameters  $\alpha_s/m_q^2 = 5.51$  GeV $^{-2}$  and  $\alpha = 0.4$  GeV are involved in  $V_{NN}(r)$ . These potentials are consistent with expectations for NN core interactions; they are repulsive and have ranges of about 1/2 fm and peak values comparable to +1 GeV, which is essentially infinite from a nuclear physics viewpoint. It may be interesting in future work to parametrize the amplitudes associated with each diagram (the weights in Table I) as a two-nucleon spin- and isospin-interaction of the form  $A I + B \vec{S}_1 \cdot \vec{S}_2 + C \vec{\tau}_1 \cdot \vec{\tau}_2 + D \vec{S}_1 \cdot \vec{S}_2 \vec{\tau}_1 \cdot \vec{\tau}_2$ , which will allow a more direct comparison with meson-exchange models [33].

Low-energy equivalent NN core potentials have been presented as the results of some of the NN resonating-group and variational calculations we discussed in the introduction. In their Figs.1 and 2 Suzuki and Hecht [34] show numerical results for the NN core potentials of Harvey [12], Faessler, Fernandez, Lübeck and Shimizu [13] and Oka and Yazaki [16]. The Faessler *et al.* and Oka-Yazaki potentials are quite similar to our potentials in Fig.1, with values at the origin between 0.6 and 1.0 GeV and comparable ranges. Harvey finds potentials with somewhat longer ranges, which Suzuki and Hecht attribute to his choice of a larger nucleon width parameter,  $b_N \equiv 1/\alpha = 0.8$  fm; the Faessler *et al.* and Oka-Yazaki values are 0.475 fm and 0.6 fm respectively, and we use a comparable  $1/\alpha = 0.493$  fm.

The NN core potentials found by Maltman and Isgur, in Fig.1 of reference [22], also have similar ranges but are somewhat larger in magnitude,  $V(0)=1.2$  GeV for I=0 and 2.3 GeV for I=1. Our difference in the contact values is due in part to the choice of parameters; in our calculations the potentials are proportional to  $\alpha_s \alpha^3/m_q^2$ , which is 0.353 GeV with our parameters and 0.489 GeV for Maltman and Isgur. Note, however, that no other reference finds the large Maltman-Isgur I=1/I=0 ratio at contact. The value chosen for  $\alpha_s \alpha^3/m_q^2$  by itself does not explain the differences between potentials; those reviewed by Suzuki and Hecht use  $\alpha_s \alpha^3/m_q^2 \approx 0.55$  GeV, so we would naively expect our potentials to be  $\approx 0.6$  times as large as theirs. Of course the values near the origin have little physical relevance due to their small Jacobean weight, and in any case we are comparing potentials derived using three different methods, and these differences may preclude a more accurate comparison of results.

The choice of parameters will be discussed in more detail in the section on differential cross sections. Here we simply note that the smaller value of  $\alpha_s$  we use is now generally preferred because recent spectroscopy studies using improved wavefunctions have considerably lowered the value required to fit hadron spectroscopy. The NN references we compare with predate the improved spectroscopy studies and thus used a rather large value of  $\alpha_s$ , which was required to give a realistic  $N\Delta$  splitting given single-Gaussian wavefunctions. We also prefer to use our fixed parameter set because these values were found to give reasonable results for low-energy S-wave  $\pi\pi$ ,  $K\pi$  and  $KN$  scattering in our previous studies [26,27,31].

Note in Fig.1 that the intermediate-range attractions which are responsible for the deuteron in I=0 and its almost-bound I=1 partner are absent from our quark Born potentials. This is as we anticipated, given that these attractions arise mainly from a spatial

distortion of interacting-nucleon wavefunctions [4,22]; in our leading-order Born calculation we assume fixed nucleon spatial wavefunctions. The attraction presumably arises at higher order in the Born series, and may be accessible through leading-order Born calculations of off-diagonal matrix elements.

Oka and Yazaki (Fig.2 of [16]) and Koike (Fig.3 of [18]) also show the S-wave phase shifts which result from their NN core interactions. In Fig.2 we show the S-wave phase shifts we find on numerically integrating the Schrödinger equation with the potentials of Fig.1. Our phase shifts are very similar to the results of these earlier resonating-group studies. Although we would like to compare our phase shifts to experiment directly, the experimental phase shifts [35] are unfortunately complicated by the presence of the deuteron and its  $I=1$  partner near threshold. These states will have to be incorporated in our calculation before we can make a useful comparison between our theoretical core phase shifts and experiment.

The Born-order approximate phase shifts (proportional to  $h_{fi}$ ) can be determined analytically using Eq.(6) of [27] and dividing by 2 for identical particles,

$$\delta^{(\ell)} = -\frac{\pi^2}{2} PE_P \int_{-1}^1 h_{fi}(\mu) P_\ell(\mu). \quad (35)$$

The momentum, energy and  $\mu = \cos(\theta_{\text{c.m.}})$  are for one nucleon in the c.m. frame. From our general result for  $h_{fi}$  (17) and the Gaussian-wavefunction integrals (28), we find an  $\ell$ th Born-order partial-wave phase shift of

$$\delta^{(\ell)} = -\frac{\alpha_s}{3m_q^2} PE_P \sum_{n=1}^8 w_n \eta_n e^{-A_n P^2} i_\ell(B_n P^2). \quad (36)$$

The spin-dependence of this result is implicit in the weights  $\{w_n\}$ . Note that these phase shifts are functions of  $\ell$  and spins only, so there is no spin-orbit force in our effective NN interaction. This is as expected given that our only interaction at the quark level is the spin-spin hyperfine term. A more realistic model will require a generalization to include the OGE spin-orbit term and perhaps coupled channel effects, as we discussed in our study of KN scattering.

The analytic Born-order result (36) for the phase shifts is unfortunately of little utility for NN S-waves given realistic quark-model parameters; the equivalent potential  $V_{NN}(r)$  is nonperturbatively large in this case, and must be iterated coherently to determine phase shifts, as we have done in Fig.2 using the NN Schrödinger equation. In contrast to this result, we previously found nonperturbative effects in the S-wave phase shifts of  $\pi\pi$ , KK and KN systems to be much less important, due to somewhat shorter-ranged forces and the smaller reduced mass. The NN Born-approximation phase shifts (36) are presumably more useful for higher partial waves and higher energies, since multiple scattering effects are expected to be largest in S-wave near threshold.

#### IV. OTHER NONSTRANGE BB' CHANNELS: N $\Delta$ AND $\Delta\Delta$

The core potentials predicted by the quark Born formalism for other nonstrange baryon-baryon channels should allow tests of the assumed hyperfine dominance in systems other than the familiar S-wave NN cases. The short-range interactions in the N $\Delta$  and  $\Delta\Delta$  channels

may be observable experimentally as final state interactions or, if the interaction is sufficiently strong to support bound states, as dibaryon molecules not far below threshold. The possibility of nonstrange resonances in the  $q^6$  sector has been considered by many authors, the earliest reference apparently being a group-theoretic study by Dyson and Xuong [36]. These  $q^6$  systems have also been studied using the bag model (which is unfortunately known to give unphysical predictions of a host of multiquark resonances), one-boson-exchange models and the nonrelativistic quark model; references before 1985 are summarised by Maltman [32].

Our results for  $N\Delta$  and  $\Delta\Delta$  are summarised by the diagram weights in Tables II and III. After completing their derivation we found that some of these matrix elements had previously been tabulated by Suzuki and Hecht [34]; our  $NN$  and  $\Delta\Delta$  weights  $w_1, w_2, w_3, w_4$  are equivalent to the coefficients  $C_{ST}^{(5)}, -C_{ST}^{(2)}, -C_{ST}^{(3)}, C_{ST}^{(4)}$  in their Table II, which provides an independent check of our results in these cases. As these weights multiply comparable spatial overlap integrals which give positive contributions to the low-energy equivalent baryon-baryon potential (34), negative weights imply attractive potential contributions.

Referring to Table II, we see that the  $N\Delta$  system has a strongly repulsive core in the channels  $I,S=2,1$  and  $1,2$  and weak core interactions in  $2,2$  and  $1,1$ . Unlike the  $\Delta\Delta$  system (to be discussed subsequently) our  $N\Delta$  core interactions do not lead to bound states in any channel. Since the lightest reported dibaryons have masses very close to the  $N\Delta$  threshold [35,37,38], the experiments may be seeing threshold effects due to the opening of the  $N\Delta$  channel, or perhaps weakly-bound  $N\Delta$  molecules. Our calculation does not support the existence of such bound states, although the  $NN$  system is similarly predicted to have a purely repulsive core, but the  $I,S=0,1$  deuteron is nonetheless bound by an intermediate-range attraction which is absent from our leading-order Born calculation. Similar weakly-bound states may exist in  $N\Delta$  and  $\Delta\Delta$  as well, despite repulsive cores.

Next we consider the  $\Delta\Delta$  system. For  $\Delta\Delta$  some general rules follow from the assumption of a single  $\lambda \cdot \lambda$  interaction; since the initial three-quark clusters are transformed into color octets by the interaction, line diagrams with zero or three pairs of quarks exchanged are forbidden. Thus the amplitude for  $\Delta^{++}\Delta^-$  elastic scattering must be zero. This implies relations between  $\Delta\Delta$  amplitudes with different isospins,

$$h_{fi}(\Delta\Delta; I = 0, S) = -h_{fi}(\Delta\Delta; I = 2, S) \quad (37)$$

and

$$h_{fi}(\Delta\Delta; I = 1, S) = -\frac{1}{9} h_{fi}(\Delta\Delta; I = 3, S) . \quad (38)$$

Specializing to the (+)-symmetry (even-L) cases in Table III, which include the S-wave channels that are *a priori* the most likely to support bound states, it is evident that two  $\Delta\Delta$  channels have strongly attractive core potentials,  $I,S=1,0$  and  $0,1$ . Of these  $0,1$  has the strongest attraction. We search for bound states by solving the Schrödinger equation in the  $\Delta\Delta$  system using the low-energy potential (34). With our reference parameter set  $\alpha_s/m_q^2 = 5.51 \text{ GeV}^{-2}$  and  $\alpha = 0.4 \text{ GeV}$  the attractive core is too weak to induce binding. Note, however, that previous studies of baryons using single-Gaussian wavefunctions have generally assumed a much stronger hyperfine term, for reasons we will discuss subsequently. If we use a typical parameter set from these references,  $\alpha_s/m_q^2 = 14.9 \text{ GeV}^{-2}$  and  $\alpha = 0.32$

GeV (Maltman and Isgur [22]), we find a single S-wave  $\Delta\Delta$  bound state in the 0,1 channel, with  $E_B = 40$  MeV. Of course this channel has a fall-apart coupling to NN, so a coupled-channel treatment including the NN system may be required to search for resonant effects. None of the other  $\Delta\Delta$  channels have sufficiently strong attractive cores to form bound states in our formalism with the Maltman-Isgur parameters.

Our result for the I,S=0,1  $\Delta\Delta$  channel is remarkably similar to the conclusion of Maltman [32], who found that the 0,1 channel has the strongest diagonal attraction in the  $\Delta\Delta$  Hilbert space, and that these diagonal forces led to a  $\Delta\Delta$  bound state with  $E_B = 30$  MeV. Maltman concluded, however, that off-diagonal effects due to the excitation of hidden-color states eliminated this bound state and led to binding in I,S=3,0 ( $E_B = 30$  MeV) and 0,3 ( $E_B = 260$  MeV) instead. The 3,0 and 0,3 channels had previously been suggested as possibilities for  $\Delta\Delta$  bound states [16,39,40]. In contrast we find strong repulsion in the 3,0 channel and a weak core in 0,3.

In view of the parameter- and approximation-dependence of predictions of  $\Delta\Delta$  bound states and the theoretical uncertainties in treating hidden-color basis states, the possibility of nonstrange dibaryon molecules should be regarded as an open question for experimental investigation. The channels which appear of greatest interest at present are the attractive-core systems I,S=0,1 and 1,0 and the 3,0 and 0,3 channels, which previous studies suggested as possibilities for binding.

## V. NN DIFFERENTIAL CROSS SECTIONS

We can use Eq.28 of reference [26],

$$\frac{d\sigma}{dt} = \frac{4\pi^5 s}{(s - 4M^2)} |h_{fi}|^2 , \quad (39)$$

to determine the nucleon-nucleon differential cross section in leading Born approximation, given the NN  $h_{fi}$  matrix element (17). For the experimentally well-determined case of unpolarised PP elastic scattering, we have a weighted sum of the S=0 and S=1 differential cross sections,

$$\frac{d\sigma}{dt} \Big|_{\text{PP,unpolarised}} = \frac{1}{4} \frac{d\sigma}{dt} \Big|_{I=1,S=0} + \frac{3}{4} \frac{d\sigma}{dt} \Big|_{I=1,S=1} . \quad (40)$$

To obtain the S=0 and S=1 cross sections one simple substitutes the appropriate I=1 diagram weights  $\{w_n\}$  from Table I and the integrals  $\{I_n\}$  from (29-31).

Before we discuss our prediction for this differential cross section we briefly recall the experimental unpolarised PP result. This is shown for a range of  $P_{\text{lab}}$  in Fig.3, adapted from Ryan *et al.* [41], Ankenbrandt *et al.* [42], Clyde *et al.* [43], Allaby *et al.* [44], and from the ISR data of Nagy *et al.* [45] and Breakstone *et al.* [46]. The data in the figure were obtained from the Durham-Rutherford HEP data archive. Near threshold the angular distribution is approximately isotropic, but as  $P_{\text{lab}}$  increases the scattering at large angles falls rapidly, and at high energies the differential cross section is dominated by an asymptotic “diffractive peak”,

$$\lim_{s \rightarrow \infty, |t|/s \ll 1} \frac{d\sigma^{\text{expt.}}}{dt} \approx ae^{bt}. \quad (41)$$

For the purely hadronic part (as distinct from the divergent forward Coulomb peak) one finds

$$a^{\text{expt.}} \approx 70 \text{ mb GeV}^{-2} \quad (42)$$

and

$$b^{\text{expt.}} \approx 11 - 12 \text{ GeV}^{-2} \quad (43)$$

for the asymptotic form [46].

On evaluating (40) for NN scattering using (17), (39) and Table I, we find that several features of the experimental differential cross section are successfully reproduced by our Born-order calculation. The theoretical Born-order cross section (40) which follows from our “reference” parameter set  $\alpha_s/m_q^2 = 5.51 \text{ GeV}^{-2}$  and  $\alpha = 0.4 \text{ GeV}$  is shown in Fig.4 for  $P_{\text{lab}} = 1.05, 1.75, 3. \text{ and } 10. \text{ GeV}$ , selected for comparison with Fig.3. Although  $P_{\text{lab}} = 10. \text{ GeV}$  superficially appears to be very relativistic, in the c.m. frame it actually corresponds to  $P_{\text{c.m.}} = 2.07 \text{ GeV}$ , which for nucleon-nucleon scattering is only quasirelativistic.

First note that the smooth evolution from an isotropic angular distribution to an asymptotic forward-peaked one with increasing  $s$  is a simple consequence of the suppression in  $s$  of all diagrams at small  $|t|$  except  $D_1$ . In our calculation the contributions of the other diagrams fall exponentially with  $s$ . The experimental large-angle scattering does not fall this rapidly, and the discrepancy is probably due to our use of single-Gaussian forms; the actual proton wavefunction has short-distance quark-quark correlations, which presumably lead to power-law contributions at large  $s$  and  $|t|$ .

Second, the observed approximate asymptotic form (41) is actually predicted by our single-Gaussian Born calculation. The overall normalization  $a$  and slope parameter  $b$  for this process are predicted to be

$$a = \frac{4\pi\alpha_s^2}{9m_q^4} \left( \frac{1}{4} (w_1^{I=1,S=0})^2 + \frac{3}{4} (w_1^{I=1,S=1})^2 \right) = \frac{6364}{19683} \frac{\pi\alpha_s^2}{m_q^4} \quad (44)$$

and

$$b = \frac{2}{3\alpha^2}. \quad (45)$$

The theoretical result (44) for the magnitude of the forward peak is actually independent of the spatial wavefunction, since the defining integral (23) is just the product of two normalization integrals in the limit  $\vec{A} = \vec{C}$ .

With the reference parameter set we predict a somewhat smaller, broader peak than is observed experimentally, with

$$a = 12. \text{ mb GeV}^{-2} \quad (46)$$

and

$$b = 4.2 \text{ GeV}^{-2} . \quad (47)$$

Both  $a$  and  $b$ , however, are sensitive to the choice of quark model parameters, and vary by factors of about 10 and 3 respectively when  $\alpha_s/m_q^2$  and  $\alpha$  are varied through a plausible range, which we shall discuss below. If we use typical ISR experimental intercept and slope values of  $a = 70. \text{ mb GeV}^{-2}$  and  $b = 11. \text{ GeV}^{-2}$  [46] as input to fix our two parameters, the fitted values are

$$\frac{\alpha_s}{m_q^2} = 13.3 \text{ GeV}^{-2} \quad (48)$$

corresponding to  $m_q = 0.21 \text{ GeV}$  if we leave  $\alpha_s = 0.6$ , and

$$\alpha = 0.246 \text{ GeV} . \quad (49)$$

Although these fitted parameters give the observed intercept  $a$  and slope  $b$ , the higher- $|t|$  wings of the resulting distribution fall much too rapidly with  $s$ . This is probably an artifact of our use of soft single-Gaussian wavefunctions, and a calculation of the differential cross sections which follow from more realistic wavefunctions will be a very interesting exercise.

The fitted strength of the hyperfine interaction (48) is now believed to be rather large, although it is similar to the values used in many previous quark-model studies of baryons. Examples of previous values in chronological order are  $\alpha_s/m_q^2 = 15.5 \text{ GeV}^{-2}$  (Oka and Yazaki, 1980 [16]);  $37.8 \text{ GeV}^{-2}$  (Harvey, 1981 [12]; this value now appears exceptionally large);  $7.7 \text{ GeV}^{-2}$  (Faessler *et al.*, 1982 [13]);  $14.9 \text{ GeV}^{-2}$  (Maltman and Isgur, 1984 [22]); and  $14.4 \text{ GeV}^{-2}$  (Koike, 1986 [18]). Large values were required to fit the  $N-\Delta$  mass splitting given single-Gaussian wavefunctions; since this is proportional to  $(\alpha_s/m_q^2)|\psi(0)|^2$ , an underestimated wavefunction at contact must be compensated for by a large  $(\alpha_s/m_q^2)$ . If one instead uses the actual Coulomb plus linear wavefunctions from the nonrelativistic Schrödinger equation with  $m_q \approx 0.3 \text{ GeV}$ , the larger value of  $|\psi(0)|$  leads to a much smaller  $\alpha_s/m_q^2 \approx 5 \text{ GeV}^{-2}$ . Since our scattering calculation uses Gaussian wavefunctions, one could argue which parameter value is most appropriate; an improved calculation with more realistic wavefunctions will probably be required to eliminate these parameter uncertainties.

The baryon width parameter  $\alpha$  has also been assigned a rather large range of values in previous work. Representative values in chronological order are  $\alpha = 0.41 \text{ GeV}$  (Copley, Karl and Obryk, baryon photocouplings, 1969 [47]);  $0.32 \text{ GeV}$  (Isgur and Karl, baryon spectroscopy, 1979 [48]);  $0.41 \text{ GeV}$  (Koniuk and Isgur, baryon photocouplings, 1980 [49]);  $0.33 \text{ GeV}$  (Oka and Yazaki, NN interactions, 1980 [16]);  $0.25 \text{ GeV}$  (Harvey, NN interactions, 1981 [12]);  $0.42 \text{ GeV}$  (Faessler *et al.*, NN interactions, 1982 [13]);  $0.25 \text{ GeV}$  (Hayne and Isgur relativised quark model, 1982 [50]);  $0.32 \text{ GeV}$  (Maltman and Isgur, NN interactions, 1984 [22]);  $0.34 \text{ GeV}$  (Koike, NN interactions, 1986 [18]);  $0.3$  and  $0.42 \text{ GeV}$ , with the smaller value preferred (Li and Close, baryon electroproduction, 1990 [51]).

Most potential models assume a value of  $m_q$  near  $0.3 \text{ GeV}$ , although the relativised models of Hayne-Isgur [50], Godfrey-Isgur [52] (mesons) and Capstick-Isgur (baryons) [53] use a lower value of  $0.22 \text{ GeV}$ . Although these relativised models also use a small value of  $\alpha_s(Q^2 = 0) = 0.6$  for the infrared limit of an effective running  $\alpha_s(Q^2)$ , the hyperfine strength  $\alpha_s(0)/m_q^2 = 12.2 \text{ GeV}^{-2}$  is again large because of the smaller  $m_q$ . Its effects are reduced, however, by the use of a “smeared” contact interaction.

The  $m_q$  and  $\alpha$  used by Hayne and Isgur are essentially identical to the values we need to fit the slope and intercept of the experimental PP diffractive peak, although this is presumably fortuitous agreement.

Although we can fit the magnitude and  $t$ -dependence of the small- $|t|$  differential cross section at high energies reasonably well with our quark Born results, we emphasize that this is at best an incomplete description of diffractive scattering, because the Born amplitude is purely real whereas the experimental small- $|t|$  amplitude is known to be close to imaginary [45,54]. This may imply that the first Born approximation is inadequate for small- $|t|$  diffractive scattering, and that the coupling to inelastic channels is an essential component of a description of the diffractive amplitude, even for elastic processes [55]. It may be necessary to iterate the effect of diagram  $D_1$  to generate the observed phase [56], perhaps including a sum over virtual inelastic channels. Our conclusion that suppression due to the spectator lines is the dominant origin of the observed diffractive  $t$ -dependence [31] would presumably be unchanged by iteration of the  $qq$  hard scattering process in diagram  $D_1$ .

In view of the complexity of the baryon-baryon scattering problem, which involves a sum of thousands of diagrams and the evaluation of 36-dimensional overlap integrals, and the questionable accuracy of our nonrelativistic single-Gaussian wavefunctions, we find our approximate agreement with experiment encouraging. The most important discrepancies are in the phase of the scattering amplitude (which may require a higher-order Born study) and in the higher- $|t|$  “wings” of the distribution, which may be more accurately described by more realistic Coulomb plus linear baryon wavefunctions. A determination of the proton-proton differential cross section given more realistic nucleon wavefunctions would be a very interesting future application of this formalism.

## VI. SUMMARY AND CONCLUSIONS

We have applied the quark Born diagram formalism to nonstrange baryon-baryon elastic scattering. In this approach the hadron-hadron scattering amplitude is taken to be the sum of all single quark-pair interactions followed by all allowed quark interchanges, with nonrelativistic quark model wavefunctions attached to the external lines. This may be a useful description of reactions which are free of  $q\bar{q}$  annihilation. The model has few parameters (here only two, the baryon oscillator parameter  $\alpha$  and the hyperfine strength  $\alpha_s/m_q^2$ , since we incorporate only the OGE spin-spin hyperfine term in this study), and with Gaussian wavefunctions and a contact interaction the scattering amplitudes can be derived analytically. The model was previously applied to  $I=2 \pi\pi$  and  $I=3/2 K\pi$  scattering with good results, and also gives reasonable results for low-energy S-wave KN scattering, although there are discrepancies at higher energies and in higher partial waves.

NN scattering is an important test of this approach because it is also annihilation-free (at the valence quark level), and the baryon wavefunction and the dominance of the spin-spin OGE hyperfine interaction in NN are already reasonably well established. We find that the quark Born diagrams predict repulsive core interactions in both S-wave NN channels, and the equivalent low-energy potentials we extract from the scattering amplitudes are very similar to the results of previous resonating-group and variational calculations. We also give results for the  $N\Delta$  and  $\Delta\Delta$  core interactions induced by the OGE spin-spin term, and find that certain  $\Delta\Delta$  channels have attractive cores and may possess bound states. Finally we

determine the NN differential cross section predicted by our Born amplitude, and compare the results with the experimental unpolarised PP differential cross section over a wide range of energies. We find that several well known features of experimental PP scattering are evident in our Born results, including the development of a high-energy forward peak with an approximately correct width and magnitude.

#### **ACKNOWLEDGMENTS**

We acknowledge useful contributions from W.Bugg, F.E.Close, G.Farrar, H.Feshbach, F.Gross, M.Guidry, N.Isgur, L.S.Kisslinger, Y.Koike, Z.Li, K.Maltman, R.J.N.Phillips, G.R.Satchler, K.K.Seth, G.Sterman, M.R.Strayer and R.L.Workman. This work was sponsored in part by the United States Department of Energy under contracts DE-AC02-76ER03069 with the Center for Theoretical Physics at the Massachusetts Institute of Technology and DE-AC05-840R21400 with Martin Marietta Energy Systems Inc, and DE-AC05-84ER40150 with SURA / CEBAF.

## REFERENCES

- <sup>1</sup> P.M.Morse, J.B.Fisk and L.I.Schiff, Phys. Rev. 50, 748 (1936); H.A.Bethe and R.F.Bacher, Rev. Mod. Phys. 8, 82 (1936), acknowledge the possibility of a potential of this general form but were skeptical, see especially Section 27, p.161; subsequent early references include G.Parzen and L.I.Schiff, Phys. Rev. 74, 1564 (1948); R.Jastrow, Phys. Rev 79, 389 (1950) and references cited therein; *ibid.*, Phys. Rev 81, 165 (1951).
- <sup>2</sup> H.Yukawa, Proc. Phys.-Mat. Soc. Japan 17, 48 (1935).
- <sup>3</sup> See for example M.Lacombe, B.Loiseau, J.M.Richard, and R.VinhMau, Phys. Rev. C21, 861 (1980); K.Holinde, Phys. Lett. C68, 121 (1981); R.Machleidt, Adv. Nucl. Phys. 19, 189 (1989); E. Hummel and J.A. Tjon, Phys. Rev. C42, 423 (1990); F.Gross, J.W.VanOrden and K.Holinde, Phys. Rev. C45, 2094 (1992).
- <sup>4</sup> N.Isgur, Acta Physica Austriaca, Suppl. XXVII, 177-266 (1985).
- <sup>5</sup> P.J.Siemens and A.S.Jensen, *Elements of Nuclei; Many-Body Physics with the Strong Interaction*, Section 2.6 (Addison-Wesley, New York, 1987).
- <sup>6</sup> C.E.DeTar, Phys. Rev. D17, 302 (1977); *ibid.*, p.323; Prog. Theor. Phys. 66, 556 (1981); *ibid.*, p.572.
- <sup>7</sup> Y.Nambu, in *Preludes in Theoretical Physics*, A.deShalit, H.Feshbach, and L.vanHove, eds. (North Holland, Amsterdam, 1966).
- <sup>8</sup> A.DeRujula, H.Georgi, and S.L.Glashow, Phys. Rev. D12, 147 (1975).
- <sup>9</sup> H.J.Schnitzer, Phys. Rev. Lett. 35, 1540 (1975).
- <sup>10</sup> D.A.Liberman, Phys. Rev. D16, 1542 (1977).
- <sup>11</sup> V.G.Neudatchin, Y.F.Smirnov, and R.Tamagaki, Prog. Theor. Phys. 58, 1072 (1977); I.T.Obukhovsky, V.G.Neudatchin, Y.F.Smirnov, and Y.M.Tchuvil'sky, Phys. Lett. 88B, 231 (1979).
- <sup>12</sup> M.Harvey, Nucl. Phys. A352, 326 (1981).
- <sup>13</sup> A.Faessler, F.Fernandez, G.Lübeck, and K.Shimizu, Nucl. Phys. A402, 555 (1983).
- <sup>14</sup> M.Harvey, J.Letourneaux, and B.Lorazo, Nucl. Phys. A424, 428 (1984).
- <sup>15</sup> C.S.Warke and R.Shanker, Phys. Rev. C21, 2643 (1980).
- <sup>16</sup> M.Oka and K.Yazaki, Phys. Lett. 90B, 41 (1980).
- <sup>17</sup> J.E.T.Ribeiro, Z. Phys. C5, 27 (1980).
- <sup>18</sup> Y.Koike, Nucl. Phys. A454, 509 (1986).
- <sup>19</sup> K.Yazaki, Nucl. Phys. A416, 87c (1984); M.Oka and C.J.Horowitz, Phys. Rev. D31, 2773 (1985); F.Lenz, J.T.Londergan, E.J.Moniz, R.Rosenfelder, M.Stingl, and K.Yazaki, Ann. Phys. (NY) 170, 65 (1986); Yu.A.Kuperin, S.B.Levin and Yu.B.Melnikov, "Generalized String-Flip Model for Quantum Cluster Scattering", Department of Mathematics and Computational Physics, St.Petersburg University report, Sec.5 (1992).
- <sup>20</sup> Z.-J.Cao and L.S.Kisslinger, Phys. Rev. C40, 1722 (1989).
- <sup>21</sup> K.Shimizu, Rep. Prog. Phys. 52, 1 (1989).
- <sup>22</sup> K.Maltman and N.Isgur, Phys. Rev. D29, 952 (1984).
- <sup>23</sup> See for example J.F.Gunion, S.J.Brodsky and R.Brankenbecler, Phys. Rev. D8, 287 (1973); S.J.Brodsky and G.R.Farrar, Phys. Rev. D11, 1309 (1975); G.P.Lepage and S.J.Brodsky, Phys. Rev. D22, 2157 (1980); G.Farrar, Phys. Rev. Lett. 53, 28 (1984); S.J.Brodsky and G.P.Lepage, in *Perturbative Quantum Chromodynamics*, ed. A.Muller (World Scientific, 1989).

<sup>24</sup> J.Botts and G.Sterman, Nucl. Phys. B325, 62 (1989); J.Botts, Nucl. Phys. B353, 20 (1991).

<sup>25</sup> N.Isgur and C.H.Llewellyn-Smith, Phys. Lett. B217, 535 (1989).

<sup>26</sup> T.Barnes and E.S.Swanson, Phys. Rev. D46, 131 (1992).

<sup>27</sup> T.Barnes, E.S.Swanson and J.Weinstein, Phys. Rev. D46, 4868 (1992).

<sup>28</sup> See for example D.Blaschke and G.Röpke, Phys. Lett. B299, 332 (1993); J.Weinstein and N.Isgur, Phys. Rev. D41, 2236 (1990); B.Masud, J.Paton, A.M.Green and G.Q.Liu, Nucl. Phys. A528, 477 (1991); and references cited therein.

<sup>29</sup> E.S.Swanson, Ann. Phys. (NY) 220, 73 (1992).

<sup>30</sup> K.Dooley, E.S.Swanson, and T.Barnes, Phys. Lett. 275B, 478 (1992); K.Dooley, University of Toronto Ph.D. thesis (1993); G.Karl, "Exotica, Survey of Exotic Mesons", in Proceedings of the Second Biennial Conference on Low Energy Antiproton Physics "LEAP '92" (Courmayeur, Italy 14-19 September 1992).

<sup>31</sup> T.Barnes and E.S.Swanson, MIT / ORNL report MIT-CTP-2169, ORNL-CCIP-92-15 (December 1992), submitted to Phys. Rev. C.

<sup>32</sup> K.Maltman, Nucl. Phys. A438, 669 (1985).

<sup>33</sup> F.Gross, personal communication.

<sup>34</sup> Y.Suzuki and K.T.Hecht, Phys. Rev. C27, 299 (1983).

<sup>35</sup> R.A.Arndt, L.D.Roper, R.L.Workman and M.W.McNaughton, Phys. Rev. D45, 3995 (1992).

<sup>36</sup> F.J.Dyson and N.-H.Xuong, Phys. Rev. Lett. 13, 815 (1964).

<sup>37</sup> M.P.Locher, M.E.Sainio and A.Svarc, Adv. Nucl. Phys. 17, 47 (1986); K.K.Seth, pp.37-68, Proceedings of the Third Workshop on Perspectives in Nuclear Physics at Intermediate Energies (Trieste, 1987), ed. S.Boffi *et al.* (World Scientific, Singapore).

<sup>38</sup> M.Aguilar-Benitez *et al.*, Phys. Lett. 170B, 1 (1986).

<sup>39</sup> T.Kamae and T.Fujita, Phys. Rev. Lett. 38, 471 (1977).

<sup>40</sup> M.Cvetič, B.Golli, N.Mankoč-Boršnik and M.Rosina, Phys. Lett. 93B, 489 (1980).

<sup>41</sup> B.A.Ryan *et al.*, Phys. Rev. D3, 1 (1971).

<sup>42</sup> C.M.Ankenbrandt *et al.*, Phys. Rev. 170, 1223 (1968).

<sup>43</sup> A.R.Clyde *et al.*, report UCRL-16275, unpublished (1966).

<sup>44</sup> J.V.Allaby *et al.*, Nucl. Phys. B52, 316 (1973).

<sup>45</sup> E.Nagy *et al.*, Nucl. Phys. B150, 221 (1979).

<sup>46</sup> A.Breakstone *et al.*, Phys. Rev. Lett. 54, 2180 (1985).

<sup>47</sup> L.A.Copley, G.Karl and E.Obryk, Nucl. Phys. B13, 303 (1969).

<sup>48</sup> N.Isgur and G.Karl, Phys. Rev. D20, 1191 (1979).

<sup>49</sup> R.Koniuk and N.Isgur, Phys. Rev. D21, 1868 (1980).

<sup>50</sup> C.Hayne and N.Isgur, Phys. Rev. D25, 1944 (1982).

<sup>51</sup> Z.Li and F.E.Close, Phys. Rev. D42, 2207 (1990).

<sup>52</sup> S.Godfrey and N.Isgur, Phys. Rev. D32, 189 (1985).

<sup>53</sup> S.Capstick and N.Isgur, Phys. Rev. D34, 2809 (1986).

<sup>54</sup> D.Bernard *et al.* (UA4 collaboration), Phys. Lett. B198, 583 (1987); P.V.Landshoff, CERN report CERN-TH.6277/91.

<sup>55</sup> R.J.N.Phillips (personal communication).

<sup>56</sup> R.G.Roberts (personal communication).

## TABLES

Table I. Diagram weights for NN elastic scattering.

	$\omega_1$	$\omega_2$	$\omega_3$	$\omega_4$	rel. phase $\omega_5 \dots \omega_8$
I=1; S=1	$\frac{59}{81}$	$\frac{17}{81}$	$\frac{17}{81}$	$\frac{10}{81}$	(-)
S=0	$\frac{31}{27}$	$\frac{7}{27}$	$\frac{7}{27}$	0	(+)
I=0; S=1	$\frac{19}{27}$	$\frac{7}{27}$	$\frac{7}{27}$	$\frac{2}{27}$	(+)
S=0	$-\frac{1}{9}$	$\frac{5}{9}$	$\frac{5}{9}$	0	(-)

Table II. Diagram weights for  $N\Delta$  elastic scattering.

	$\omega_1$	$\omega_2$	$\omega_3$	$\omega_4$	$\omega_5$	$\omega_6$	$\omega_7$	$\omega_8$
I=2; S=2	$\frac{7}{9}$	$\frac{1}{9}$	$-\frac{5}{9}$	0	$\frac{2}{9}$	$\frac{2}{9}$	$-\frac{4}{9}$	$-\frac{1}{3}$
S=1	$\frac{37}{27}$	$\frac{7}{27}$	$\frac{1}{27}$	$-\frac{4}{27}$	$-\frac{2}{27}$	$-\frac{2}{27}$	$\frac{4}{27}$	$-\frac{1}{27}$
I=1; S=2	$\frac{13}{27}$	$\frac{7}{27}$	$\frac{1}{27}$	0	$-\frac{2}{27}$	$-\frac{2}{27}$	$\frac{4}{27}$	$\frac{1}{9}$
S=1	$\frac{7}{81}$	$\frac{49}{81}$	$-\frac{29}{81}$	$-\frac{28}{81}$	$\frac{2}{81}$	$\frac{2}{81}$	$-\frac{4}{81}$	$\frac{1}{81}$

Table III. Diagram weights for  $\Delta\Delta$  elastic scattering.

	$\omega_1$	$\omega_2$	$\omega_3$	$\omega_4$	rel. phase $\omega_5 \dots \omega_8$
I=3; S=3	1	-1	-1	1	(-)
S=2	$\frac{5}{3}$	$-\frac{1}{3}$	$-\frac{1}{3}$	-1	(+)
S=1	$\frac{19}{9}$	$\frac{1}{9}$	$\frac{1}{9}$	$-\frac{1}{9}$	(-)
S=0	$\frac{7}{3}$	$\frac{1}{3}$	$\frac{1}{3}$	1	(+)
I=2; S=3	$\frac{1}{3}$	$-\frac{1}{3}$	$-\frac{1}{3}$	$\frac{1}{3}$	(+)
S=2	$\frac{5}{9}$	$-\frac{1}{9}$	$-\frac{1}{9}$	$-\frac{1}{3}$	(-)
S=1	$\frac{19}{27}$	$\frac{1}{27}$	$\frac{1}{27}$	$-\frac{1}{27}$	(+)
S=0	$\frac{7}{9}$	$\frac{1}{9}$	$\frac{1}{9}$	$\frac{1}{3}$	(-)
I=1; S=3	$-\frac{1}{9}$	$\frac{1}{9}$	$\frac{1}{9}$	$-\frac{1}{9}$	(-)
S=2	$-\frac{5}{27}$	$\frac{1}{27}$	$\frac{1}{27}$	$\frac{1}{9}$	(+)
S=1	$-\frac{19}{81}$	$-\frac{1}{81}$	$-\frac{1}{81}$	$\frac{1}{81}$	(-)
S=0	$-\frac{7}{27}$	$-\frac{1}{27}$	$-\frac{1}{27}$	$-\frac{1}{9}$	(+)
I=0; S=3	$-\frac{1}{3}$	$\frac{1}{3}$	$\frac{1}{3}$	$-\frac{1}{3}$	(+)
S=2	$-\frac{5}{9}$	$\frac{1}{9}$	$\frac{1}{9}$	$\frac{1}{3}$	(-)
S=1	$-\frac{19}{27}$	$-\frac{1}{27}$	$-\frac{1}{27}$	$\frac{1}{27}$	(+)
S=0	$-\frac{7}{9}$	$-\frac{1}{9}$	$-\frac{1}{9}$	$-\frac{1}{3}$	(-)